Supporting Information

Probing Multi-Phased Transition in Bulk MoS_2 by Direct Electron Injection

Krishna P Dhakal,[§#] Ganesh Ghimire,[§#] Kyungwha Chung,[§#] Dinh Loc Duong,[†,§*] Sung Wng Kim,[§*] and Jeongyong Kim[§*]

[§]Department of Energy Science, Sungkyunkwan University, Suwon 16419, Republic of Korea.

[†]Center for Integrated Nanostructure Physics, Institute for Basic Science, Suwon 16419, Republic of Korea.

[#]K. P. D., G. G. and K. C. contributed equally to this work.

*Correspondence Authors: ddloc@skku.edu, kimsungwng@skku.edu, j.kim@skku.edu

Table of Contents:

1. Raman spectra of pristine and oxidized dicalcium nitride crystals.
2. Layer number dependent PL and Raman spectra of MoS_2 films.
3. Theoretical evidence of phonon softening in the MoS_2 crystal due to degenerate electron doping.
4. Thickness estimation of the MoS_2 crystal placed on a $[Ca_2N]^+\cdot e^-$ substrate.
5. Assignment of Raman peak positions of $MoS_2/[Ca_2N]^+\cdot e^-$ heterostructures.
6. Doping density-dependent Raman peak positions of monolayer 1T' MoS_2 obtained from theoretical calculations.
7. Raman spectrum of the thin MoS_2 crystal placed on a $[Ca_2N]^+\cdot e^-$ substrate.
8. Polarization-dependent Raman vibrational modes of 2H MoS_2.
9. Differential reflectance measurement from the pristine MoS_2 and $MoS_2/[Ca_2N]^+\cdot e^-$ heterostructures

S1: Raman spectra of pristine and oxidized dicalcium nitride crystals

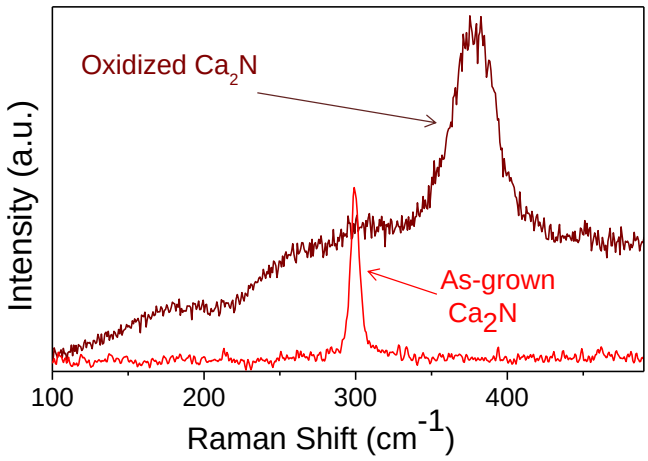

Figure S1: Raman spectra of pristine (red curve) and oxidized (brown curve) $[Ca_2N]^+ \cdot e^-$ crystals. If $[Ca_2N]^+ \cdot e^-$ crystals are exposed to air, they undergo rapid oxidation and lose their electron-doping ability.

S2: Layer number dependent PL and Raman spectra of MoS_2 films

Figure S2 A displays the PL spectra obtained from MoS_2 crystals of different thicknesses including mono-, bi-, and a few layers (~8L). The corresponding optical contrasts are shown in the inset of Figure S2 a. It is noted that gap changes in the indirect bandgap position was much higher when the layer number varied from 2L to 4L than the gap change observed along the direct transition (K-K), thus rendering the different rate of bandgap variation in direct and indirect gap positions as a function of layer number, which help us to distinguish the layer number and thickness (Figure S2 b). Layer-number dependency could also be observed in the Raman vibrational modes as illustrated in Figure S2 c and d. Distinct in-plane (E_{2g}^1) and out-of-plane (A_{1g}) phonon modes are characteristic features of the hexagonal lattice structure of MoS_2 crystals; they are observed at 385 and 404 cm^{-1} in 1L MoS_2. With an increase in MoS_2 thickness (>1L), a gradual (a) red-shift in the E_{2g}^1 Raman mode, (b) blue-shift in the A_{1g} Raman mode, and (c) linearly increasing frequency differences between the E_{2g}^1 and A_{1g} modes could be observed (Figure S2 d). Therefore, crystal thickness up to 4 to 5 layers could be unambiguously identified using thickness-dependent PL spectra, Raman peak positions, and their frequency differences as the reference. Beyond 4 to 5 layers, thickness-dependent characterization using optical PL and Raman spectra becomes difficult. Our results on layer thickness-dependent PL and Raman spectra are consistent with previously reported results on MoS_2 crystals. [1,2]

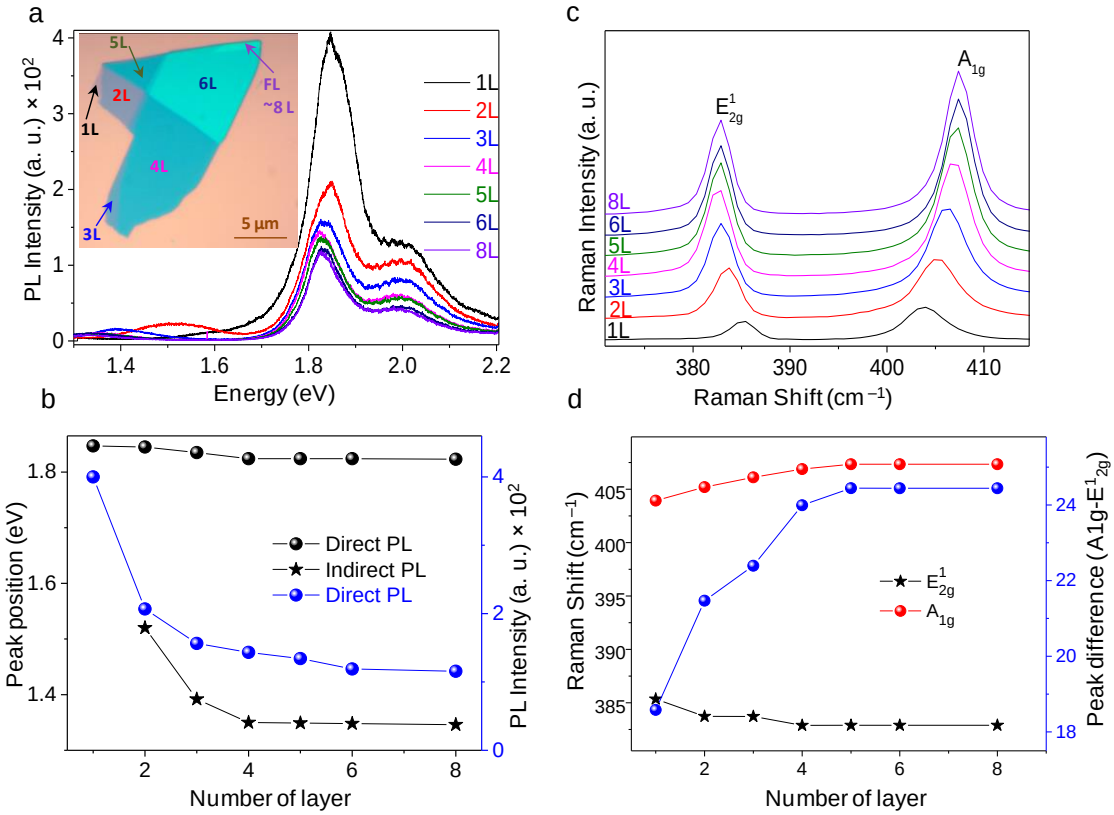

Figure S2: Layer number-dependent PL and Raman spectra of MoS_2. (**a**) PL spectra of MoS_2 from 1L to 8L. The inset displays the optical images of samples of different layer thicknesses. (**b**) Peak-position and peak-intensity comparison of direct and indirect PL emission spectra obtained from samples with different number of layers. (**c**) Layer number-dependent Raman spectra. (**d**) Plot of peak position and peak difference of the in-plane phonon mode (E_{2g}^1) and out-of-plane phonon mode (A_{1g}). All measurements were conducted at an excitation energy of 2.41 eV (514.5 nm laser).

S3 and S4: Theoretical evidence of phonon softening in the MoS_2 crystal due to degenerate electron doping

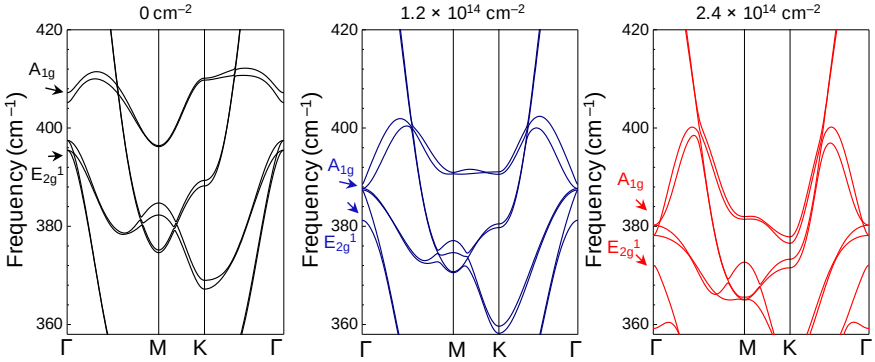

Carrier Density cm^{-2}	E_{2g}^1(R) cm^{-1}	A_{1g} (R) cm^{-1}
0	397.5	407.2
2.5×10^{13}	395.2	401.8
5×10^{13}	393.6	399.8
1.2×10^{14}	387.4	381.2
2.4×10^{14}	378.1	359.2

Figure S3: Doping density-dependent phonon dispersion relationships calculated for 2L-MoS_2. The table on the right shows a comparison of Raman-frequency softening for the E_{2g}^1 and A_{1g} modes with respect to the doped electron density.

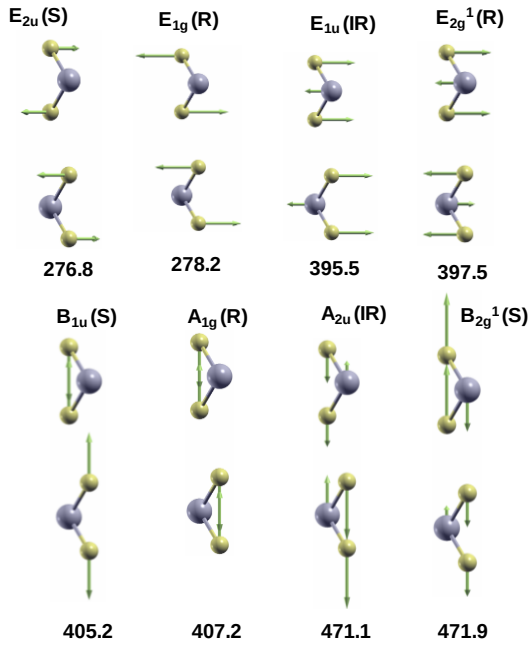

Figure. S4: Raman vibrational modes used for calculating the results shown in Fig. S3 for 2H 2L-MoS_2. Each frequency modes are expressed in cm^{-1}.

S5: Thickness estimation of the MoS_2 crystal placed on a $[Ca_2N]^+ \cdot e^-$ substrate

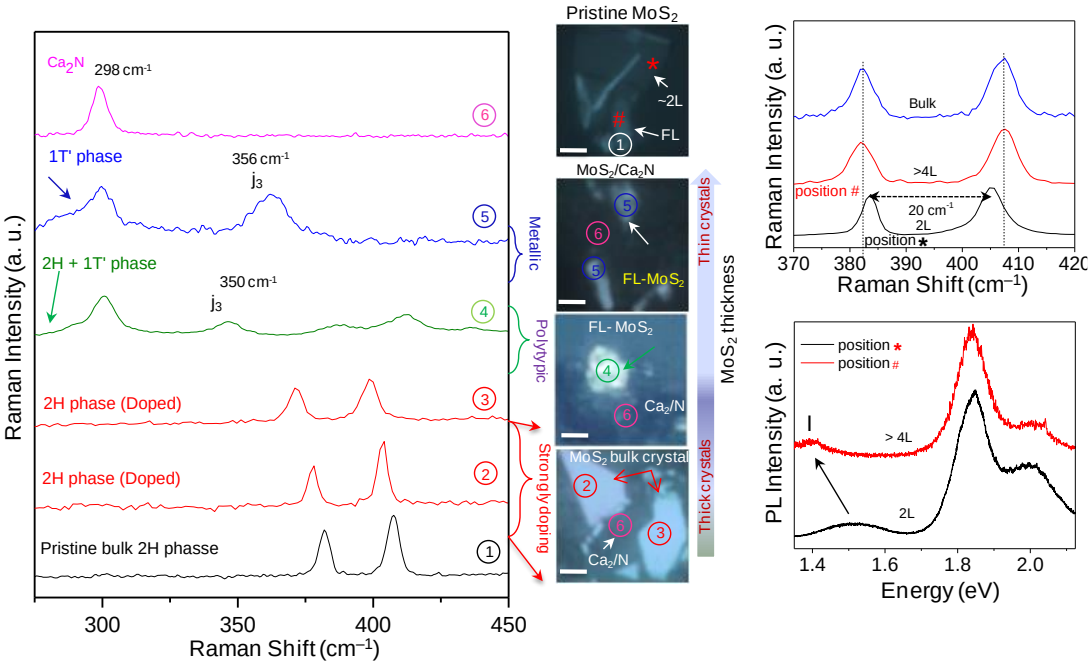

Figure S5: Empirical estimation of the thickness of $MoS_2/[Ca_2N]^+ \cdot e^-$ heterostructures. Raman spectra of pristine bulk (black curve, labeled as 1) and $MoS_2/[Ca_2N]^+ \cdot e^-$ heterostructures prepared using various thickness of MoS_2 crystals (bulk to few-layer, labeled 2 through 5). The spectra are shifted vertically for clarity. Observation of the typical Raman mode of $[Ca_2N]^+ \cdot e^-$ at 298 cm^{-1} in spectra 4 and 5 ensures that the corresponding MoS_2 flake must be thinner than those which showed Raman spectra with 2H phase Raman modes (spectra 2 and 3) in the heterostructure. The optical images shown on the right represent typical heterostructures of MoS_2 crystals of various thicknesses and the locations at which the corresponding Raman spectra were taken. The scale bar is 5 µm. Raman-mode softening and the emergence of new Raman modes explains the transition of MoS_2 into a metallic phase in terms of the reduction in layer thickness. The PL and Raman spectra at the right confirm that the pristine few-layer sample indicated by the symbol "#" is in the limit of the bulk structure,[1,2] which indicates that metallic structures exhibiting spectra 4 and 5 can also be counted as thinner bulk structures (~5–10 nm).

S6: Raman spectrum of the thin MoS_2 crystal placed on a $[Ca_2N]^+ \cdot e^-$ substrate

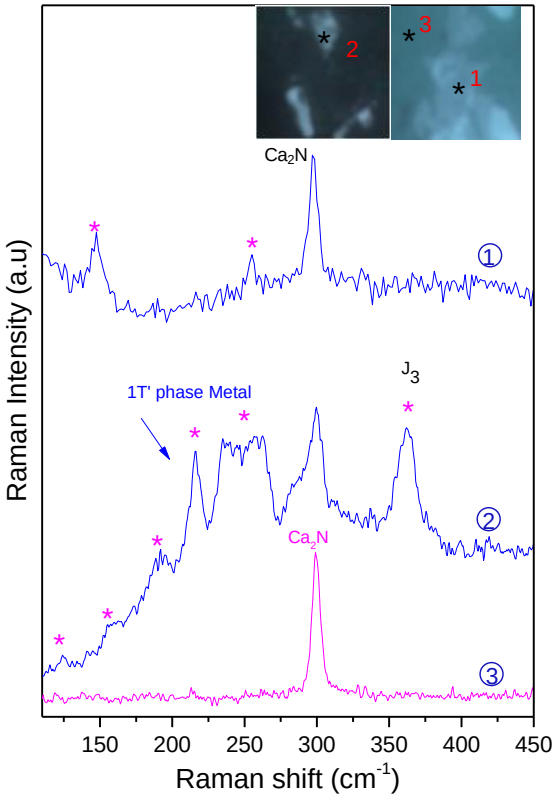

Figure S6: Raman spectra of the thinnest MoS_2 on 2D-$[Ca_2N]^+ \cdot e^-$ (spectrum 1) among our samples. Raman spectrum of a thicker bulk MoS_2 on 2D-$[Ca_2N]^+ \cdot e^-$ (spectrum 2) is shown for comparison. The intensity of the 2D-$[Ca_2N]^+ \cdot e^-$ Raman mode in the spectrum 1 is almost the same as pristine 2D-$[Ca_2N]^+ \cdot e^-$ indicating that the thickness of this particular MoS_2 is only a few nanometers.

Table S1: Assignment of Raman peak positions of $MoS_2/[Ca_2N]^+ \cdot e^-$ heterostructures. R and IR represent Raman- and infrared-active modes, respectively.

Our experimental $[Ca_2N]^+ \cdot e^-/MoS_2$		Peaks in 2H MoS_2		Peaks in 1T′ MoS_2		Assignment
Peaks in the 2H + 1T′ phase (cm^{-1})	Peaks in the 1T′ metallic phase (cm^{-1})	Experimental (cm^{-1}) [1-9]	Theoretical (cm^{-1}) [9-11]	Experimental (cm^{-1}) [6, 12-15]	Theoretical (cm^{-1}) [11, 16-18]	
138	142	-	-	-	140	A_g (R)
167	160	-	-	156	152, 175	B_g (J_1) R
184	-	-	177	-		A_{1g} (M)-LA (M) (R)
198	192	-	-	192		E_{1g} (R)
212	215	-	-	216	212	A_g (R)
236	236, 259	-	-	226	226	B_g (J_2) (R)
290	285	-	287	287	286, 288	E_u + E_{1g} (IR + R)
350	358	-	-	333, 358	333, 355	A_g (J_3) (R)
-	-	383	383	-	-	E_{2g}^1 (R)
392	-	-	393	-	-	E_{1u} (IR)
-	-	408	408	408	403	A_{1g} (R)
415, 420	415	421	419	-	412	B_{2g}^2 + E_{1u}^2 (IR + R)
440	-	-	427	-	-	E_{2g}^2 (R)
454	452	464	466	-	-	2LA (M) (R)
535	-	528	529	-	-	E_g (M) + TA’ (M) (R)
564	-	571	572	-	-	2 × E_{1g} (R)
653	-	643	641	-	-	A_{1g} (M) + LA’ (M) (R)
693	-	-	699	-	-	B_{3g} (R)

Table S2: Doping density-dependent Raman peak positions of monolayer 1T' MoS_2 obtained from theoretical calculations. R and IR represent Raman- and infrared-active modes, respectively.

Experimental $[Ca_2N]^+ \cdot e^-/MoS_2$ peaks in 1T′ metallic phase (cm^{-1})	Theoretical Raman peaks in 1T′-MoS_2 (cm^{-1})				Previous theoretical results on 1T′-MoS_2 [11, 16-18]	
	0 cm^{-2}	1.1×10^{14} cm^{-2}	2.2×10^{14} cm^{-2}	Peak assignment	Raman Peak position (cm^{-1})	Peak assignment
142	145.7	147.6	142.3	A_g (R)	140	A_g (R)
160	156.6	164.6	167.7	B_g (R)	152, 175	B_g (J_1) R
192	219.2	203.5	207.4	B_g (R)	-	-
215	219.2	214.2	209.0	A_g (R)	212	A_g (R)
236, 259	226.5,	234.2,	233.2,	A_u (IR),	226	B_g (J_2) (R)
259	247.6, 267.1	248.7, 264.1	249.4, 261.2	B_u (IR), B_u (IR)	-	-
285	280.6, 281.5, 283.0	277.1, 281.0, 287.2	274.5, 284.0, 289.3	A_g (R), B_g (R), A_u (IR)	286, 288	$E_u + E_{1g}$ (IR + R)
358	330.5, 338.6, 345.4	326.5, 337.6, 343.9	323.3, 338.1 343.6	A_g (R), B_u (IR), A_g (R)	333, 355	A_g (J_3) (R)
415	402.2	400.4	403.0	A_g (R)	403, 412	A_{1g} (R), $B_{2g}^2 + E_{1u}^2$ (IR + R)
452	462.5	461.5	463.0	B_u (IR)	-	-

S7: Polarization-dependent Raman vibrational modes of 2H MoS_2

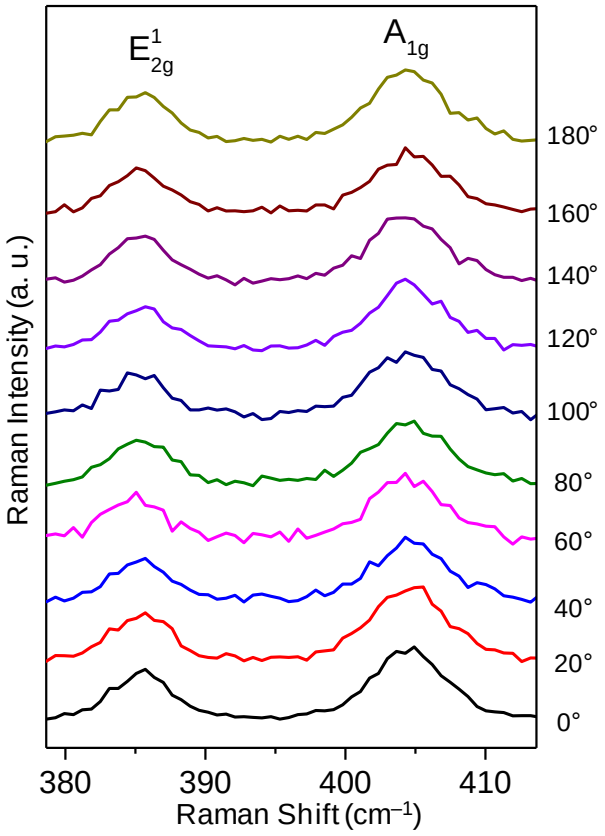

Figure S7: Polarization-dependent Raman spectra of monolayer 2H MoS_2. Raman spectra at different sample rotation angles were measured with a fixed analyzer and polarizer parallel to each other. The in-plane (E_{2g}^1) Raman mode showed a constant intensity at all polarization angles. The hexagonal symmetry of MoS_2 results in an isotropic in-plane response with respect to the polarization of incident light. Our results on the isotropic nature of the 2H crystal agree with previously reported results on MoS_2 characterized by polarized Raman spectroscopy.[3,17]

S8: Differential reflectance measurement from the pristine MoS_2 and $MoS_2/[Ca_2N]^+\cdot e^-$ heterostructures

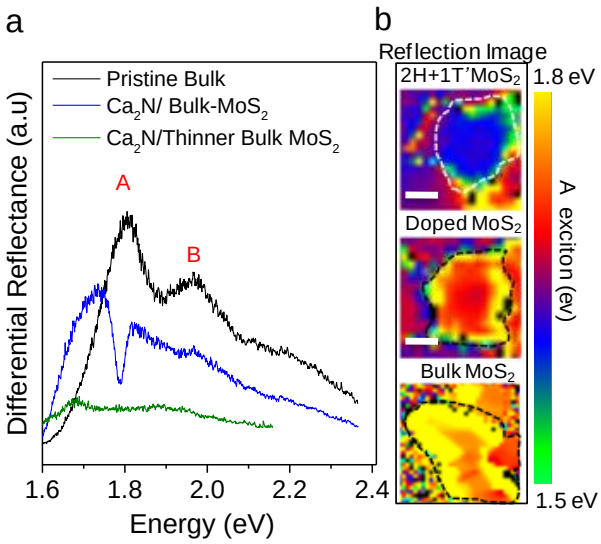

Figure S8: (a) Differential Reflectance measurement of the pristine MoS_2 and $MoS_2/[Ca_2N]^+\cdot e^-$ heterostructure. (b) Spectral mapping images of corresponding samples are shown. The diferential reflectance measurement was performed by preparing the sample on the transparent glass. Detail of the spectral mapping technique is described in the Ref. 2.

REFERENCES

1. Mak, K. F.; Lee, C.; Hone, J.; Shan, J.; Heinz, T. F. Atomically Thin MoS_2: a New Direct-Gap Semiconductor. *Phys. Rev.Lett*. **2010**, *105*, 136805.
2. Dhakal, K. P.; Duong, D. L.; Lee, J.; Nam, H.; Kim, M.; Kan, M.; Lee , Y. H.; Kim, J. Confocal Absorption Spectral Imaging of MoS_2: Optical Transitions Depending on the Atomic Thickness of Intrinsic and Chemically Doped MoS_2. *Nanoscale* **2014**, *6*, 13028−13035.

3. Xia, M.; Li, B.; Yin, K.; Capellini, G.; Niu, G.; Gong, Y.; Zhou, W.; Ajayan, P. M.; Xie, Y. H. Spectroscopic Signatures of AA′ and AB Stacking of Chemical Vapor Deposited Bilayer MoS_2. *ACS Nano* **2015**, *9*, 12246−12254.
4. Lin, M. L.; Tan, Q. H.; Wu, J. B.; Chen, X. S.; Wang, J. H.; Pan, Y. H.; Zhang, X.; Cong, X.; Zhang, J.; Ji, W.; Hu, P. A.; Liu, K. H.; Tan, P. H. Moiré Phonons in Twisted Bilayer MoS_2. *ACS Nano* **2018**, *12*, 8770−8780.
5. Stacy, A. M.; Hodul, D. T. Raman Spectra of IVB and VIB Transition Metal Disulfides Using Laser Energies Near The Absorption Edges. *J. Phys. Chem. Solids* **1985**, *46*, 405-409.
6. Jiao, Y.; Mukhopadhyay, A.; Ma, Y.; Yang, L.; Hafez, A. M.; Zhu, H. Ion Transport Nanotube Assembled with Vertically Aligned Metallic MoS_2 for High Rate Lithium-Ion Batteries. *Adv. Energy Mater.* **2018**, *8*, 1702779.
7. Zheng, W.; Zhu, Y.; Li, F.; Huang, F. Raman Spectroscopy Regulation in van der Waals Crystals. *Photonics Res.* **2018**, *6*, 991−995.
8. Wu, H.; Yang, R.; Song, B.; Han, Q.; Li, J.; Zhang, Y.; Fang, Y.; Tenne, R.; Wang, C. Biocompatible Inorganic Fullerene Like Molybdenum Disulfide Nanoparticles Produced by Pulsed Laser Ablationin Water. *ACS Nano* **2011**, *5*, 1276−1281.
9. Mignuzzi, S.; Pollard, A. J.; Bonini, N.; Brennan, B.; Gilmore, I. S.; Pimenta, M. A.; Richards, D.; Roy, D. Effect of Disorder on Raman Scattering of Single-Layer MoS_2.*Phys. Rev B: Condens. Matter Mater. Phys.* **2015**, *91*, 195411.
10. Frey, G. L.; Tenne, R.; Matthews, M. J.; Dresselhaus, M. S.; Dresselhaus, G. Raman and Resonance Raman Investigation of MoS_2Nanoparticles. *Phys. Rev B: Condens. Matter Mater. Phys.***1999**, *60*, 2883−2892.
11. Livneh, T.; Spanier, J. E. A Comprehensive Multiphonon Spectral Analysis in MoS_2. *2D Mater*. **2015**, *2*, 035003.

12. Tan, S. J. R.; Abdelwahab, I.; Ding, Z.; Zhao, X.; Yang, T.; Loke, G. Z. J.; Lin, H.; Verzhbitskiy, I.; Poh, S. M.; Xu, H.; Nai, C. T.; Zhou, W.; Eda, G.; Jia, B.; Loh, K. P.Chemical Stabilization of 1T′ Phase Transition Mmetal Dichalcogenides with Giant Optical Kerr Nonlinearity. *J. Am. Chem. Soc.* **2017**, *139*, 2504−2511.
13. Chi, Z. H.; Zhao, X. M.; Zhang, H.; Goncharov, A. F.; Lobanov, S. S.; Kagayama, T.; Sakata, M.; Chen, X. J. Pressure-Induced Metallization of Molybdenum Disulfide. *Phys. Rev. Lett.* **2014**, *113*, 036802.
14. Nayak, A. P.; Pandey, T.; Voiry, D.; Liu, J.; Moran, S. T.; Sharma, A.; Tan, C.; Chen, C. H.; Li, L. J.; Chhowalla, M.; Lin, J. F.; Singh, A. K.; Akinwande, D. Pressure-Dependent Optical and Vibrational Properties of Monolayer Molybdenum Disulfide. *Nano Lett.* **2015**, *15*, 346−353.
15. Yin,X.; Wang,Q.; Cao, L.; Tang, C. S.; Luo,X.; Zheng, Y.; Wong,L. M.; Wang, S. J.; Quek, S. Y.; Zhang,W.; Rusydi, A.; Wee, A. T. S.Tunable Inverted Gap in Monolayer Quasi-Metallic MoS_2 Induced by Strong Charge-Lattice Coupling. *Nat. Commun.* **2017**, *8*, 486.
16. Fisher, H. First-Principles Investigation of Electron-Phonon Interactions in Novel Superconductors, *Ph.D. Thesis*, Oxford University, Oxford , UK, **2014**.
17. Zhang, X.; Qiao, X. F.; Shi, W.; Wu, J. B.; Jiang, D. S.; Tan, P. H. Phonon and Raman Scattering of Two-Dimensional Transition Metal Dichalcogenides From Monolayer, Multilayer to Bulk Material. *Chem. Soc. Rev.* **2015**, *44*, 2757−2785.
18. Calandra, M. Chemically Exfoliated Single-Layer MoS_2: Stability, Sattice Dynamics, and Catalytic Adsorption From First Principles. *Phys. Rev. B: Condens. Matter Mater. Phys.* **2013**, *88*, 245428.